Aerodynamically Optimal Regional Aircraft Concepts: Conventional and Blended Wing-Body Designs

Thomas A. Reist* and David W. Zingg†

Institute for Aerospace Studies, University of Toronto

4925 Dufferin St., Toronto, Ontario, M3H 5T6, Canada

The blended wing-body represents a potential revolution in efficient aircraft design, yet little work has explored the applicability of this design concept to small aircraft such as those that serve regional routes. We thus explore the optimal aerodynamic shape of both a blended wing-body and conventional tube-and-wing regional aircraft through high-fidelity aerodynamic shape optimization. A Newton-Krylov solver for the Euler and Reynolds-Averaged Navier-Stokes (RANS) equations is coupled with a gradient based optimizer, where gradients are calculated via the discrete adjoint method. Both the conventional and blended wing-body regional jets are optimized for a 500nmi mission at Mach 0.8 with the objective of minimizing drag subject to a trim constraint. Both Euler and RANS-based optimization is performed, with the result of the Euler optimization forming the starting point for the RANS-based optimization. Several optimization problems are considered with variation of sections, twist and planform. Root bending moment is constrained as a surrogate for structural weight in cases with planform variations. The optimized blended wing-body presented here exhibits a lift-to-drag benefit of 30% over a conventional design similar to existing regional aircraft. Changes in planform that result in aerodynamically optimal conventional and blended wing-body designs give a 21% lift-to-drag advantage to the blended wing-body.

Nomenclature

x, y, z	Streamwise, spanwise and vertical coordinates
b	Total aircraft span
c	Local chord length
MAC	Mean aerodynamic chord
S	Reference planform area
V	Volume
t/c	Section thickness normalized with local chord length
q_∞	Freestream dynamic pressure
C_L, C_D, C_M	Lift, drag and pitching moment coefficients of the entire aircraft
c_l	Sectional lift coefficient
L/D	Lift-to-drag ratio
AoA	Aircraft angle-of-attack
W	Aircraft weight at start of cruise
MTOW	Maximum take-off weight
OEW	Operating empty weight
C_p	Coefficient of pressure
Subscript	
0	Original value

*Ph.D. Candidate, AIAA Student member, tom.reist@utoronto.ca

†Professor and Director, Canada Research Chair in Computational Aerodynamics and Environmentally Friendly Aircraft Design, J. Armand Bombardier Foundation Chair in Aerospace Flight, Associate Fellow AIAA, dwz@oddjob.utias.utoronto.ca

I. Introduction

With increasing oil prices and concern about both the exhaustion of fossil fuels and their contribution to climate change, the need for more fuel efficient aircraft is becoming more pronounced for both economic and environmental reasons. Although there have been great advances in transport aircraft efficiency since the introduction of the de Havilland Comet in 1952, the conventional tube-and-wing (CTW) configuration remains to this day. Performance improvements have come from modifications to aerodynamic design, such as the use of winglets and supercritical airfoils, as well as high performance materials and increasingly fuel efficient engines. However a step change in fuel efficiency may be realized through novel configurations. One such configuration that has received much attention in recent years is the blended-wing-body (BWB). This design combines the aircraft fuselage and wings into one tightly integrated airframe with improved aerodynamic, structural, propulsive, and acoustic efficiency.

The BWB has the potential to be more aerodynamically efficient than conventional configurations for several reasons. For a given internal volume, the BWB has less wetted surface area, leading to a better lift-to-drag ratio.[1] It has also been shown to be more area-ruled than conventional designs, which allows for reduced wave drag and potentially higher cruise speeds.[1] The overall shape of the BWB is also cleaner than a conventional design, leading to reduced interference drag. Structurally, the aerodynamic lifting loads are more closely aligned with the weight of the aircraft due to the lifting fuselage, leading to reduced bending loads in the main wing structure and therefore lower structural weight.[1] The use of a well integrated propulsion system, such as boundary-layer-ingestion or distributed propulsion, can lead to propulsive efficiencies. A well integrated propulsion system on the top of the aircraft can also provide significant noise reductions due to the acoustic shielding provided by the aerodynamic surfaces.[2] The highly integrated nature of the design allows for efficiency improvements; however this also increases the design challenges stemming from such a highly coupled configuration.

One of the main structural challenges associated with the BWB is the lack of the efficient cylindrical pressure vessel present in conventional designs. Much work has been dedicated to the design of efficient composite structures tailored for handling these pressure loads.[3–5] Due to its tailless nature, stability and control can be challenging with this design. Work has been done on addressing some of these issues,[6,7] With such a radically different design, certification and customer acceptance must also be addressed. Finally, perhaps the biggest obstacle to the development of the BWB is the financial risk associated with pursuing such a novel design. However, as rising fuel prices continue to reduce operating profits, the potential benefits of this unconventional design may justify its development.

Several large projects around the world have focused on the development of the BWB design. In the United States, Boeing and NASA have been involved in the identification and development of enabling technologies required for the BWB design,[1,3,6,8–10] with contributions leading to the X-48 flight demonstrators. A BWB design focused on noise reduction has been developed as part of Cambridge and MIT's 'Silent' Aircraft Initiative.[2,11] In Europe, two of the main projects relating to BWB design are the Multidisciplinary Optimization of a Blended Wing Body (MOB)[12] and the Very Efficient Large Aircraft (VELA)[13] projects.

Aerodynamic shape optimization (ASO) has been applied to the BWB design at a variety of fidelity levels. Peigin and Epstein[14] used a Navier-Stokes solver and genetic optimizer for the optimization of the MOB configuration for multiple operating points with airfoil, dihedral and twist design variables. Qin et al.[15] performed spanload optimization through twist modification as well as 3D surface optimization using both Euler and Navier-Stokes solvers. Both airfoil and sweep optimization were performed by Le Moigne and Qin[16] using a discrete adjoint method with an Euler solver. They demonstrated that the imposition of pitching moment constraints has a large impact on the optimal shape yet only a small performance penalty must be paid. The performance improvements obtained using Euler-based optimization are also realized when evaluated with a Navier-Stokes solver. The challenge of considering stability and control of flying-wings during aerodynamic shape optimization has been addressed by Mader and Martins[17] through the application of a time-spectral method for optimizing in the presence of static and dynamic stability constraints. A small BWB was optimized by Kuntawala et al.[18] using a large number of geometric design variables for full 3D surface optimization. More recently, Lyu and Martins optimized an 800 passenger BWB using both the Euler[19] and RANS[20] equations subject to trim, static-stability, and root bending-moment constraints. Previous work by Reist and Zingg includes single and multipoint optimization of a regional jet class BWB using both the Euler and RANS equations.[21] The impact of trim and stability constraints on the optimal BWB design at both on- and off-design conditions was examined. It was demonstrated that, for cruise, these constraints lead to a small performance penalty at on-design conditions through tailoring of the

aerodynamic shape and aircraft weight distribution, while performance degrades significantly at off-design conditions.

Historically, the focus of BWB design investigations has been on large capacity aircraft in the 400-1000 passenger range. The BWB's intrinsic design features lend themselves well to large aircraft. However this design may also offer advantages in the regional jet segment. Nickol examined a series of BWB aircraft ranging from 98-400 passengers.[9] As expected, the fuel burn benefit was most significant for the larger aircraft, with the 98 passenger aircraft burning more fuel than a comparable tube-wing aircraft. However, the fuel burn disadvantage of the small BWB was highly sensitive to drag. Thus, if a suitable drag reduction can be achieved through aerodynamic shape optimization, the BWB could potentially be more fuel efficient than the tube-wing aircraft for a variety of aircraft classes. The objective of this paper is to compare aerodynamically optimal versions of the two configurations for a regional jet class aircraft.

II. Methodology

The aerodynamic shape optimization algorithm used comprises three main components: 1) a multiblock Newton-Krylov solver for the Euler and Reynolds-Averaged Navier-Stokes (RANS) equations, 2) a B-spline geometry parameterization which is coupled with a linear elasticity mesh movement strategy, and 3) the gradient-based optimizer SNOPT with gradients calculated using the discrete adjoint method.

The flow solver is a multiblock finite-difference solver which uses summation-by-parts operators for spatial discretization and simultaneous approximation terms for the imposition of boundary conditions and block interface conditions. The Krylov subspace method Generalized Minimum Residual (GMRES) is used with approximate Schur preconditioning for the solution of the discrete equations. The one-equation Spalart-Allmaras turbulence model is used for the modeling of turbulent flows. Details of the flow solver can be found in Hicken and Zingg[22] and Osusky and Zingg.[23]

At each optimization iteration for which a geometric shape change occurs, the computational grid must be moved to reflect this change. To accomplish this, each block of the computational grid is fitted with a B-spline volume. As the B-spline control points on the aerodynamic surface are moved by the optimizer, each B-spline volume block is treated as a linear elastic solid, for which a finite-element solution is obtained to define the new shape of the B-spline volume. The computational grid is then recovered from this new B-spline volume. This method has been found to be very robust for large shape changes while being computationally inexpensive. Details can be found in Hicken and Zingg.[24]

Due to the high cost of evaluating the flow equations, a gradient-based optimizer is used for optimization, as gradient-based optimizers typically require fewer function evaluations than genetic algorithms.[25] The penalty paid is that for multimodal optimization problems only a local optimum may be found. This can be addressed using the gradient-based global optimization techniques proposed by Chernukhin and Zingg.[26] The gradients of the objective and constraints are evaluated using the discrete adjoint method. This method is advantageous for problems with many design variables, as the cost of the gradient evaluation is nearly independent of the number of design variables. The number of adjoint solutions required is proportional to the number of objectives and constraints which depend on the flow properties. Since this can contribute to significant computational cost for practical problems an efficient method of solving the linear system of the adjoint problem is required. For this, a modified flexible version of the Generalized Conjugate Residual with Orthogonalization and Truncation (GCROT) algorithm is used.[27] The gradient-based optimizer SNOPT is used, as it allows for the solution of large-scale constrained problems. Details of the adjoint method and its integration with the flow solver and mesh movement are given by Hicken and Zingg[24] while the details of SNOPT are described by Gill et al.[28]

The above algorithm has been used extensively for ASO of various geometries including induced drag minimization of non-planar wings,[29] optimization of wings in turbulent flows,[30] the investigation of the multimodality of ASO problems[26] and the optimization of conventional aircraft[31] and BWB[18,21] aircraft.

III. Baseline Design

Both aircraft concepts are intended to serve as regional jets with a single-class capacity of approximately 100 passengers, while having a maximum range capability of 2000nmi with 100nmi reserves. Since most regional jets are not flown at their maximum range for most missions,[32] optimization is performed for a single-stage 500nmi flight at Mach 0.80 and 40,000ft with 100nmi reserves for both designs. While such a

high cruise altitude for a short range mission would have air traffic management and structural implications, these are not considered here.

Both the BWB and CTW baseline designs are developed using a low-fidelity tool that incorporates aerodynamic and weight-and-balance analysis using the methods of Roskam,[33] Torenbeek,[34] and Raymer.[35] For the BWB design, the weight of the center body structure is obtained using the method of Bradley.[36] The remaining structure, systems, fuel and operational item weights of the BWB are assumed to be similar to those of CTW aircraft. The same aerodynamic models are used for both aircraft, with the BWB being treated simply as a wing. Details of each design are presented below. All weight estimates are based on current technology levels. This weight estimation methodology has been evaluated for both a series of CTW designs against publicly available data, and for BWB aircraft against the results of Nickol.[9a] We stress that the methods used to choose the mission profiles and to develop the baseline designs are very low-fidelity and do not represent full system optimal design or operation. Instead, they are meant only to serve as a reasonable starting point for the high-fidelity optimization. Higher fidelity methods such as those of Liem et al.[37] shall be applied in the future to better represent the full system optimum. From the basic geometric information provided by the low-fidelity design, a full surface model is created using the geometry toolbox developed by Gagnon and Zingg.[31]

A. Conventional Tube-and-Wing Design

The baseline CTW design is modeled after in-service aircraft such as the Bombardier CRJ1000 and Embraer E190 using publicly available data. The fuselage is sized such that it can fit all passengers in a 4-abreast configuration as well as all crew, monuments (lavatories, galleys, etc) and baggage. Engines are mounted on the aft fuselage. The size and position of the wing and horizontal stabilizer are chosen both to be representative of in-service designs as well as to offer reasonable wing- and tail-loading values. The wing and tail use the NASA SC(2)-0414 and SC(2)-0010 airfoils,[38] respectively. Estimates for aircraft weight and performance are obtained via the methods described above. The resulting baseline design is shown in Figure 2 with information given in Table 1. Note that the engines and vertical stabilizer are included in the conceptual design (thus contributing to the drag and weight build-ups) however they are not modeled during the high fidelity optimization, as reflected by their absence from Figure 2.

B. Blended-Wing-Body Design

With no in-service BWB aircraft to serve as a reference, the baseline BWB is designed primarily via the conceptual design methods described above. The first step in generating the geometric shape is to size the cabin such that it fits all passengers, crew, aisles and monuments so as to produce a shape that can be well integrated into the rest of the airframe in order to avoid unnecessary structural weight and wetted surface area. As in many BWB concepts[1,2,9,36] a 'home plate' shaped cabin is utilized. The length of the outboard cabin wall is defined via the required cabin height (plus an allowance for structure space), and the airfoil thickness at the corresponding spanwise location. The width of the cabin is increased by adding seats until the required number of seats, aisles and monuments are accommodated. Appropriately sized cargo holds are added outboard of the passenger compartment. The cabin layout is shown in Figure 1. The remainder of the airframe is designed around this cabin via an iterative procedure, with the aim of avoiding unnecessary surface area and excessive structural weight. The body uses custom airfoils which are designed primarily to accommodate the cabin, and the wing uses the SC(2)-0414 section.[38] The baseline design is shown in Figure 3 with information given in Table 2.

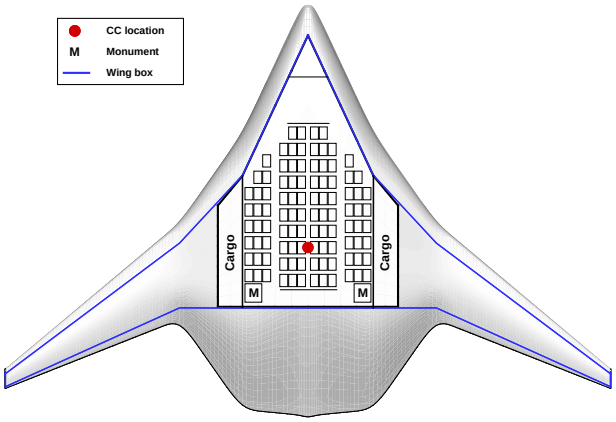

Figure 1: BWB cabin and primary structure layout.

[a]Advanced technology factors similar to those used by Nickol are included when evaluating weights for comparison with his results.

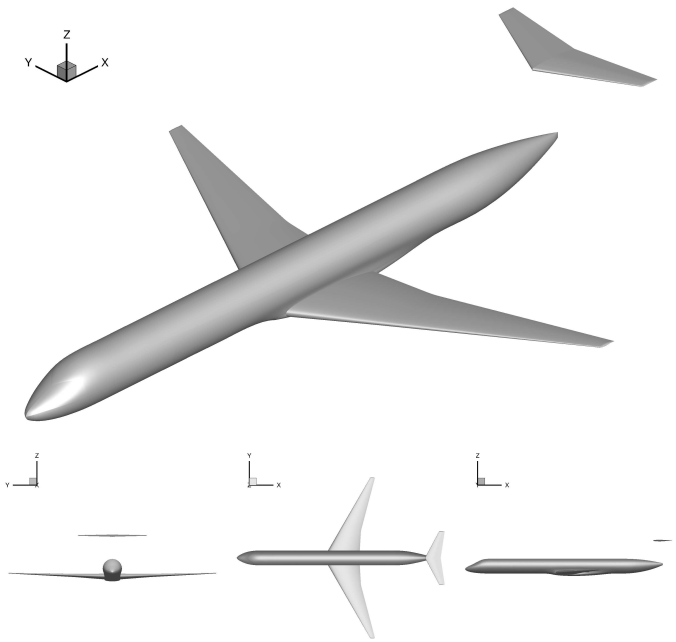

Figure 2: Baseline CTW design geometry.

Capacity	
Passengers	100
Crew	5
Max payload	24,000 lb
Geometry	
Reference area	1062.0 ft^2
Total span	96.8 ft
Length	118.4 ft
MAC	13.5 ft
Aspect ratio	8.8
Weight	
MTOW	103,250 lb
OEW	61,050 lb
Wing load at MTOW	97.2 lb/ft^2
Nominal mission cruise	
Range	500 nmi
Altitude	40,000 ft
Mach number	0.80
Reynolds number*	21 $\times 10^6$
C_L†	0.49
CG location‡	66 ft

* Based on wing MAC

† At start of cruise

‡ Measured from aircraft nose.

Table 1: Baseline CTW design summary.

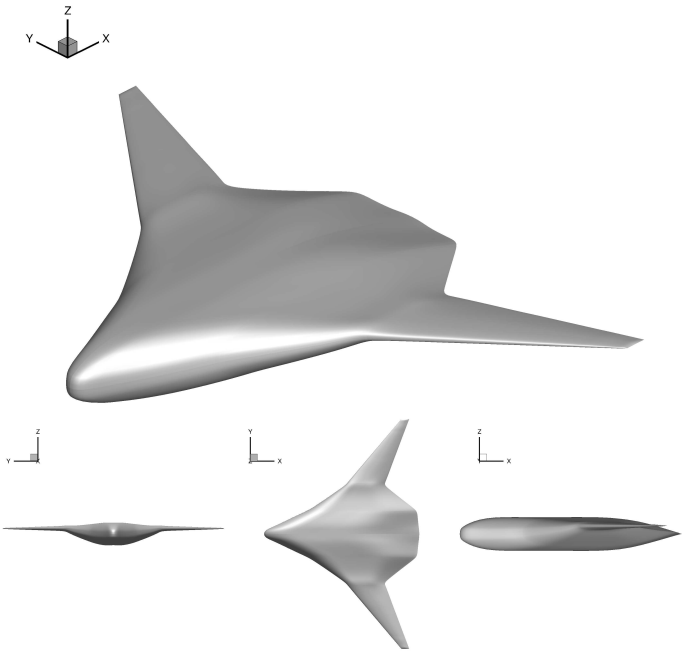

Figure 3: Baseline BWB design geometry.

Capacity	
Passengers	100
Crew	5
Max payload	24,000 lb
Geometry	
Reference area	2368.9 ft^2
Total span	98.5 ft
Length	68.8 ft
MAC	40.5 ft
Aspect ratio	4.1
Weight	
MTOW	108,100 lb
OEW	66,400 lb
Wing load at MTOW	45.6 lb/ft^2
Nominal mission cruise	
Range	500 nmi
Altitude	40,000 ft
Mach number	0.80
Reynolds number*	62 $\times 10^6$
C_L†	0.23
CG location‡	42 ft

* Based on wing MAC

† At start of cruise

‡ Measured from aircraft nose.

Table 2: Baseline BWB design summary.

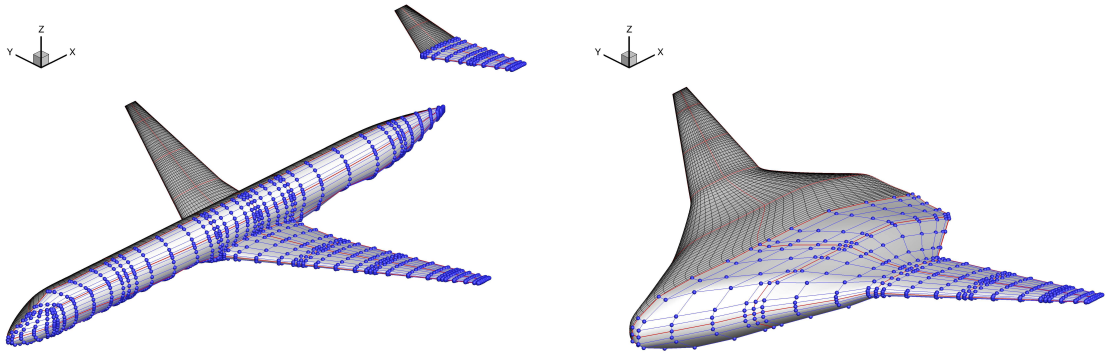

(a) Baseline CTW surface grids

(b) Baseline BWB surface grids

Figure 4: Surface CFD grid (black) and B-spline control grid (blue) on the baseline designs. B-spline control points are marked by the blue spheres, and red edges denote grid block boundaries. (Not to scale.)

IV. Aerodynamic Shape Optimization

The CTW design uses a 620 block grid with 4.2×10^6 nodes for solutions of the Euler equations, and 9.7×10^6 nodes for solution of the RANS equations. In order to resolve the boundary-layer in the RANS solution, an average off-wall spacing of 1.5×10^{-6}MAC ($y^+ \approx 1.0$ at design conditions) is used on the RANS grids. The BWB uses a 168 block grid with 1.5×10^6 nodes for Euler solves, and a 3.9×10^6 node grid for RANS solutions with an average off-wall spacing of 5×10^{-7}MAC ($y^+ \approx 1.0$ at design conditions.) Both geometries have the same grid resolution on the surface, i.e. the same number and distribution of nodes in the chord-wise, span-wise and wall-adjacent normal directions. The use of structured multiblock grids together with the complexity of the CTW geometry compared to that of the BWB results in the larger number of blocks and hence grid size for the CTW geometry, even though both grids have similar resolution on the surface. Figure 4 shows both the surface CFD, and B-spline control grids on the baseline CTW and BWB designs.

A. Design Variable Definition

The B-spline parameterization of the CFD grid provides not only a robust method of mesh movement as described in Section II, but the B-spline control points that lie on the aerodynamic surface provide a means by which the optimizer can control the geometry. However, the x, y, z coordinates of these control points have little direct relation to features of interest such as twist, span, dihedral, etc. Thus, a set of design variables is used which provides a method of defining the location of these control points through intuitive design variables. The B-spline control points are assigned to 'regions', where a region is selected based on a common role. For example, a single region might include all control points inboard of the wing crank, a second could form outboard of the crank, and a third could form a winglet. Each of these regions has its own local coordinate system. Within this coordinate system design variables including local chord, twist, section shape, dihedral, sweep, and leading/trailing edge shape are defined. The location of a given region is a function of the location and shape of the regions inboard of it. Having different portions of the wing defined in their own coordinate system as opposed to the global coordinate system allows better control of the local shape. For example, using the z control point coordinates to control the section shape works well for a wing with small dihedral angles, but provides little practical control for the airfoil sections of a winglet. In the cases presented here, the CTW main wing has two regions, one inboard and one outboard of the crank as well as a separate region which controls the tail. The BWB has one region which forms the body, and one region which forms the wing.

On the CTW, in addition to the region design variables which control the wing shape, the incidence angle of the wing and tail are also variables. The tail angle is required in order to trim the aircraft, while the wing angle allows the optimizer to find the optimal loading of both the wing and fuselage. Since the wing is mounted on the fuselage, changes in wing incidence angle, root chord, and root section require that the fuselage surface can adapt to these changes to maintain a water-tight geometry at the fuselage-wing junction. In order to accomplish this, the control points on the fuselage are moved based on the movement

of the control points at the wing root via an algebraic perturbation similar to that used by Leung and Zingg for CFD mesh movement[39] of the form

$$\mathbf{x}_k = \mathbf{x}_k^0 + (\mathbf{x}_1 - \mathbf{x}_1^0)\left[\frac{1+\cos(\pi S_k)}{2}\right]^\beta \qquad \text{for} \quad k = 2 \ldots k_{\max} \tag{1}$$

where $\mathbf{x}$ is the 3-vector of control point coordinates, and k is the control point index along control mesh grid lines emanating from the wing root. The case of $k = 1$ corresponds to the control points at the fuselage-wing junction that are controlled by design variables on the first wing region. The '0' superscript corresponds to the geometry at the start of the optimization. S_k is the normalized arc-length along a given control mesh line emanating from the wing root and is given by

$$S_k = \frac{\sum_{i=2}^{k} ||\mathbf{x}_i^0 - \mathbf{x}_{i-1}^0||}{\sum_{i=2}^{k_{\max}} ||\mathbf{x}_i^0 - \mathbf{x}_{i-1}^0||} \tag{2}$$

where $k_{\max}$ is the number of control points along the fuselage over which the propagation is to occur. The parameter β is used to control the degree to which geometric changes at the fuselage-wing junction propagate along the fuselage. Large values are desirable as they localize fuselage shape changes to near the fuselage-wing junction, yet they can lead to self-intersection of the fuselage surface for large wing root geometry changes. A value of $\beta = 4$ serves as a good compromise for the typical level of wing root geometric deformations.

B. Optimization Cases

Several trim-constrained drag minimization problems are considered; the design variables and constraints of each are summarized in Table 3. In all cases the angle-of-attack of the aircraft is a design variable, as are the wing and tail incidence angles relative to the fuselage for the CTW cases. In Case 1 the wing and tail of the CTW are free to twist, while for the BWB both the body and wing can twist. The sections of the BWB body and wing and those of the CTW wing are free. In Cases 2 and 3 the span and taper of the wing are free for both the CTW and BWB in addition to the variables of Case 1. In the CTW cases the root chord length is fixed. Each case must satisfy lift and pitching moment constraints in order to achieve a trimmed design. In addition, the polyhedron shown in Figure 5 forms a constraint that prevents the aerodynamic surface of the BWB's body from encroaching upon the required cabin space. In each case the wing volume is constrained such that the required 4500gal of fuel occupies no more than 80% of the enclosed wing volume as per Raymer.[35] In Case 2 the planform area is constrained to that of the initial geometry. In total there are between 495 and 497 design variables for each case. Since the span is variable in Cases 2 and 3, a root bending moment constraint is imposed such that the root bending moment cannot exceed that of the Case 1 optimal design. This is intended to act as a surrogate for a structural model such that the aerostructural trade-offs of the induced drag decrease due to increasing the span and the associated weight penalty are captured. Thus, to a low-fidelity approximation, the structural weight of the optimized wing between each case is constant for both configurations. The optimization presented herein models only the aerodynamic performance of the clean design. Thus structural, stability and control, low-speed, maneuver, aeroelastic, propulsion, operational and certification issues are not considered beyond the level previously mentioned. For stability considerations of a similar regional jet BWB see Reference 21. However, both the CTW and BWB optimization problems make the same assumptions with the aim that the optimization result reflects a proper comparison of the aerodynamic performance of the two designs at the primary design condition.

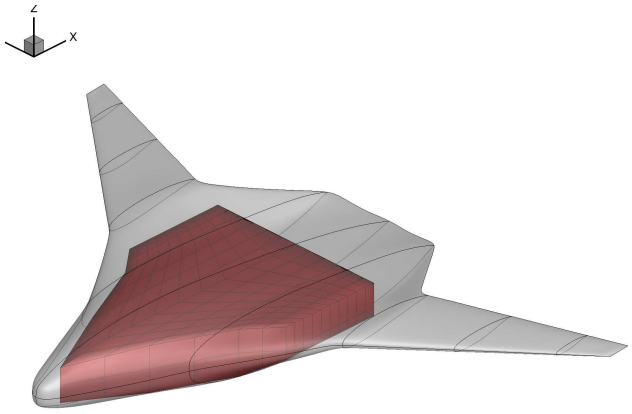

Figure 5: Polyhedron forming the cabin shape constraint.

Table 3: Design variables and constraints. Not all variables/constraints are applicable to all cases. Bounds given as percentages represent deviation from the initial values.

	CTW			BWB		
Variables	$-3^\circ \leq$	AoA	$\leq +3^\circ$	$-3^\circ \leq$	AoA	$\leq +3^\circ$
	$-3^\circ \leq$	Wing incidence	$\leq +3^\circ$			
	$-10^\circ \leq$	Tail incidence	$\leq +10^\circ$			
	$-5^\circ \leq$	Wing twist	$\leq +5^\circ$	$-5^\circ \leq$	Wing twist	$\leq +5^\circ$
	$-5^\circ \leq$	Tail twist	$\leq +5^\circ$	$-5^\circ \leq$	Body twist	$\leq +5^\circ$
	$-5\% \leq$	Sections*	$\leq +5\%$	$-5\% \leq$	Sections*	$\leq +5\%$
	$-50\% \leq$	Span	$\leq +50\%$	$-50\% \leq$	Span	$\leq +50\%$
Constraints	$-25\% \leq$	t/c	$\leq +50\%$	$-25\% \leq$	t/c	$\leq +50\%$
	$1.25V_{\text{fuel}} \leq$	V_{wing}		$1.25V_{\text{fuel}} \leq$	V_{wing}	
		$S = S_0$			$S = S_0$	
					Cabin shape	
		$L = W$			$L = W$	
		$C_M = 0$			$C_M = 0$	

* The amount, in percentage of local chord, by which the control points defining the sections can move normal to the chordline.

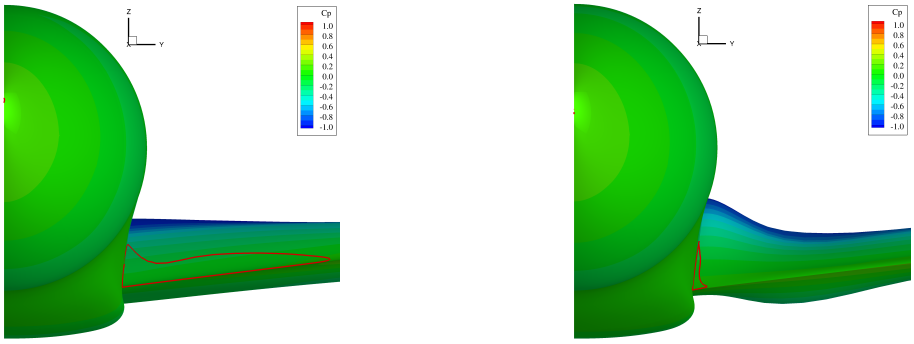

(a) Euler-optimized CTW analyzed with RANS

(b) Case 1 optimized CTW

Figure 6: Wing trailing edge at the wing-body junction of the CTW showing regions of separated flow outlined in red.

V. Optimization Results

Since the conceptual design of each baseline geometry does not provide a detailed aerodynamic shape, an Euler based optimization is performed which allows the quick determination of a design that is shock-free and has an aerodynamically optimal spanwise load distribution. This Euler-based optimization forms the starting point for the RANS-based optimization. Having a starting point that is shock-free eases the RANS solution process, leading to shorter run times. Thus, for each configuration an Euler-based version of Case 1 is performed. In the Euler design space both configurations are trimmed at the upper angle-of-attack bound of 3.0°. When analyzed with RANS the BWB satisfies the lift target at 4.8° and the CTW is trimmed at 4.0°. While this Euler-based optimization achieves a shock-free and nearly elliptically loaded wing, when analyzed using the RANS equations these features are lost. Shocks reappear on both configurations and significant regions of separated flow form on the CTW (shown in Figure 6a), as well as the BWB to a lesser extent. These two features change the local c_l and thus the elliptical lift distribution achieved in the Euler-based optimization is lost. While the Euler-optimized designs do not perform well when analyzed with RANS, they still perform significantly better than the original unoptimized designs, which exhibit even stronger shocks and larger separated regions.

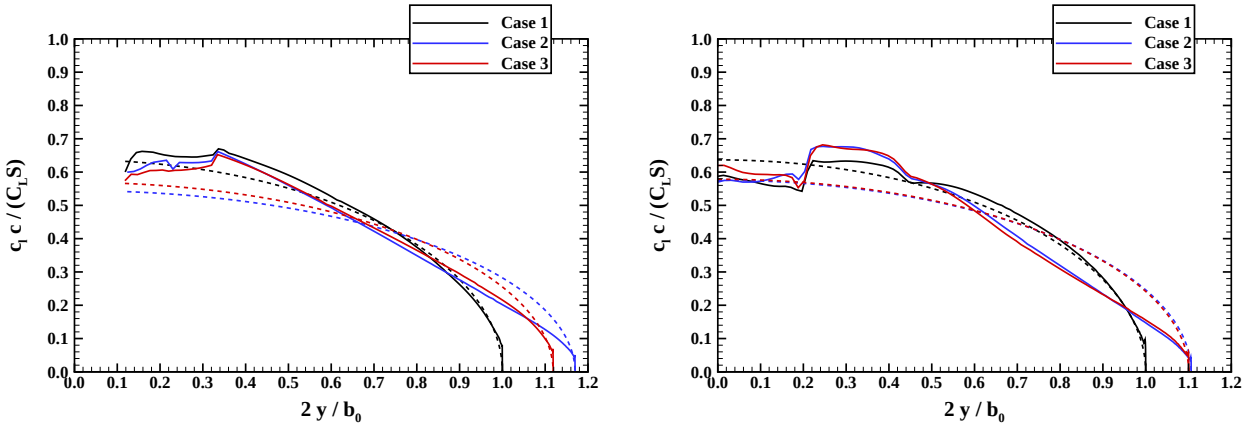

(a) CTW wing lift distributions

(b) BWB lift distributions

Figure 7: Spanwise lift distributions on each optimized design with the corresponding elliptical distribution shown with a dashed line of the corresponding colour.

Table 4: Performance summary of the RANS-optimized designs.

		AoA	C_L	C_M	C_D	L/D
Case 1	CTW	3.00°	0.490	0.00	0.0386	12.7
	BWB	2.57°	0.230	0.00	0.0139	16.5
Case 2	CTW	3.00°	0.490	0.00	0.0353	13.9
	BWB	3.00°	0.230	0.00	0.0137	16.8
Case 3	CTW	3.00°	0.534	0.00	0.0379	14.1
	BWB	3.00°	0.234	0.00	0.0138	17.0

A. Case 1: Twist and section optimization

The first case holds the planform constant while varying the airfoil sections and geometric twist. The resulting lift distributions and sectional pressure distributions for the CTW and BWB cases are shown in Figures 7 and 8 respectively. For both the CTW and BWB cases, the spanwise lift distribution is nearly elliptical on the wing, while for the BWB case the elliptical shape is lost on the centerbody due to the imposition of the cabin shape and trim constraints. The sectional pressure distributions in Figure 8 show that both designs are shock free, and separation is nearly eliminated. The CTW case is trimmed with a tail incidence angle of -2.2°, while the BWB is trimmed by fore-loading the centerbody, as seen from the C_p distributions at $2y/b = 0.00$ and $2y/b = 0.20$ in Figure 8b, such that all of the lift on the centerbody is generated ahead of the center of gravity. The separation present on the Euler-optimized shapes is nearly eliminated as seen in Figure 6b. As described in Section A, for the CTW optimization problems the optimizer has no direct control over the wing-body fairing shape, only the section shape at the wing-body junction. Thus, the optimizer forms a highly contoured wing at the wing-body junction, seen in Figure 6b, in order to control the pressure recovery and eliminate the separation. A similar shape occurs in each RANS-based optimization case. The BWB's t/c distribution is relatively constant for each optimization case, with the thickness up to near 40% span being determined by the cabin shape constraint, and that from 50-70% going to the lower bound. In no case does the BWB wing volume reach its lower bound. The performance of the optimized designs, given for each case in Table 4, shows a 30% benefit in the lift-to-drag ratio for the BWB compared to the CTW configuration. The friction and pressure drag contributions are broken down in Table 5.

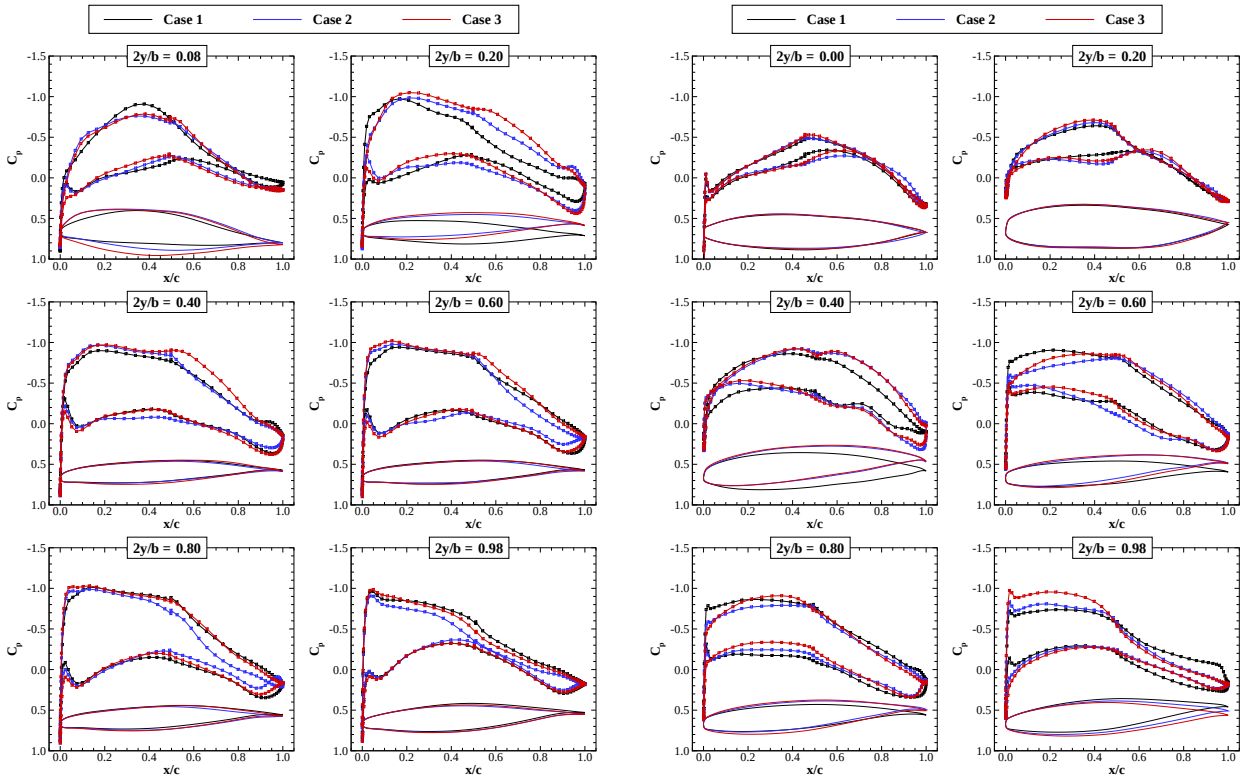

(a) Optimized CTW sectional pressure distributions.

(b) Optimized BWB sectional pressure distributions.

Figure 8: Sectional pressure distributions on each optimized design.

Table 5: Breakdown of pressure and friction drag for each RANS-optimized design.

		D/q_∞ [ft^2]	D_p/q_∞ [ft^2]	D_f/q_∞ [ft^2]
Case 1	CTW	41.0	19.1	21.9
	BWB	33.3	18.5	14.8
Case 2	CTW	37.3	16.5	20.8
	BWB	32.7	17.9	14.8
Case 3	CTW	36.8	16.9	19.9
	BWB	32.5	18.0	14.5

B. Case 2: Twist, section and planform optimization with fixed bending moment

Adding variations in span with a constraint on the root bending moment allows the optimizer to trade the benefit of increased span with the resulting decrease in span efficiency due to the deviation from an elliptical lift distribution. In order to maintain a constant area, changes in span must be accompanied by changes in the chord distribution. This affects the local boundary-layer development and hence viscous drag. For both CTW and BWB cases, the root bending moment is constrained to be no greater than that produced by the Case 1 optimal design. The bending moment constraint is applied at the wing root, which for the BWB is where the wing meets the centerbody (at approximately 40% span.) The planform chosen by the optimizer is shown in Figure 9. The span has increased by 17% for the CTW and 10% for the BWB. The resulting lift distributions are shown in Figure 7 where the decrease in tip loading required to meet the bending target is evident. Due to the increased span in the BWB case and the resulting aft movement of the center of pressure due to the wing sweep, more fore-loading and some aft-loading is seen on the centerbody in Figure 8b which

is used to maintain trim. As in Case 1, the design is shock-free and separation is nearly absent. The CTW wing volume reaches its lower bound in this case due to the smaller chords than in Case 1. The CTW t/c distribution is similar to that of Case 1 except at the wing root where the optimizer takes advantage of the larger fixed chord to best utilize the increased thickness in order to satisfy the volume constraint and allow the rest of the wing to remain thin. The resulting performance displayed in Tables 4 and 5 shows that for the CTW case a 9% drag benefit is realized from increasing the span with most of this decrease coming from reduction in pressure drag, which includes induced drag. The benefit for the BWB case is less pronounced with a 2% benefit. For both the CTW and BWB optimization cases the optimizer finds the optimal trade-off between induced and viscous drag due to planform changes while not exceeding the root bending moment target. The CTW optimization is able to reduce induced drag through a 17% span increase while simultaneously reducing friction drag due to a reduction in wetted area. The optimal drag trade-off for the BWB occurs with a 10% span increase yielding a reduction in induced drag, with little change in friction drag. Even though the change in span benefits the CTW design more than the BWB, the BWB still has a 21% lift-to-drag advantage over the CTW.

C. Case 3: Twist, section, planform, and area optimization with fixed bending moment

While wing area is typically determined by off-design requirements such as take-off, we investigate the potential benefit at cruise that results from changing the planform without the constraint on area. This allows the optimizer more freedom to achieve an optimal benefit by trading-off induced and viscous drag. As in Case 2 the root bending moment is constrained. For the CTW case the span is increased by 12% with a corresponding 10% decrease in planform area. This increases the induced drag relative to Case 2 but lowers friction drag, as shown in Table 5, for a small net benefit over Case 2. As in Case 2 the CTW wing volume goes to its lower bound with a large t/c at the wing root. For the BWB case, the optimized result is very similar to that of Case 2, as seen from the planform in Figure 9 and the lift distribution in Figure 7b. The area is reduced by 2% which leads to a slight increase in induced drag and decrease in friction drag for a small net drag benefit over the Case 2 BWB result. The differences between the Case 2 and 3 lift-to-drag ratios are near the level of accuracy one may expect from the grids being used and for the depth to which the optimizer is being converged, particularly for the BWB which has only a small difference between the Case 2 and 3 geometries. Thus, conclusions about the performance differences between Cases 2 and 3 should be made with care.

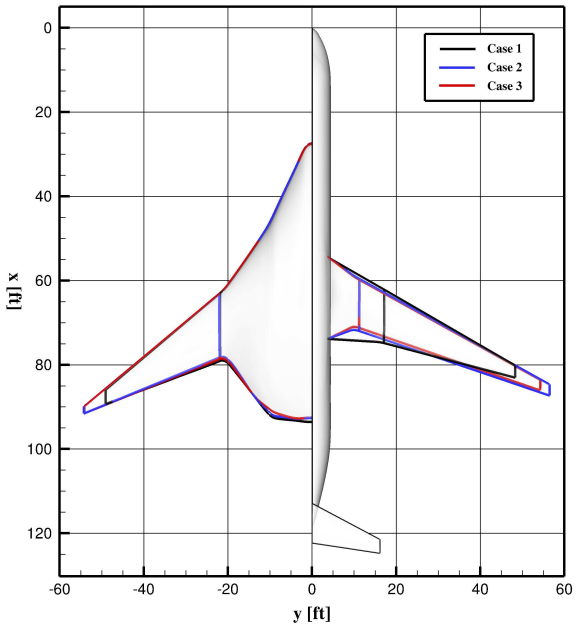

Figure 9: Planform of each optimized design.

D. Effect of grid resolution

The drag values presented above are higher than would be expected for CTW and BWB aircraft. It is believed that this is due to the fact that the solutions are not grid converged. For example, when the Case 1 optimized BWB is analyzed with a three times finer grid the lift-to-drag ratio increases from 16.5 to 19.1, an increase of 16%, although this is still not a grid converged solution. This difference has been found to be consistent between both the Euler-optimized design when analyzed with RANS and the RANS-optimized design as the grid is refined, thus justifying the use of coarser grids to capture the optimized benefit. While no RANS grid refinement studies of the optimized CTW configuration are available, induced drag scaling from Euler-based grid refinement studies indicate a similar trend between BWB and CTW induced drag with grid refinement. Hence we expect the benefit of the BWB relative to the CTW to be maintained once grid converged results are available.

VI. Conclusions

Both Euler and RANS-based aerodynamic shape optimization has been applied to the design optimization of a conventional tube-and-wing (CTW) and a blended wing-body (BWB) regional jet. With geometric twist and sections as design variables, in addition to the wing and tail incidence angles on the CTW design, a lift-to-drag benefit of 30% is obtained by the BWB compared to the aerodynamically optimized CTW whose planform is similar to regional jets currently in service. When the optimizer is permitted to change the span of both the CTW and BWB such that the aerodynamic optimum (in the presence of a root bending constraint) can be found, the BWB exhibits a 21% lift-to-drag benefit over the CTW, with the increase in span benefitting the CTW more so than the BWB. The lift-to-drag values of the CTW and BWB are lower than expected, likely caused by the fact that the solutions are not grid converged. The lift-to-drag ratio for the optimal BWB increased by 16% when analyzed on a somewhat finer mesh. Nevertheless, it is expected that the lift-to-drag ratio improvement associated with the BWB will persist when computations are performed on finer grids. While preliminary, this work suggests that, as with the extensively studied high-capacity/long-haul class of BWB, significant improvements in aerodynamic efficiency can be obtained by this unconventional concept in the regional jet segment. Only on-design conditions are studied in this work, yet off-design performance is important and shall be considered through multipoint optimization in the future. Future work shall include the application of this same optimization framework to problems with more geometric design variables and to optimization considering a wider range of operating conditions. In order to evaluate and compare these configurations thoroughly, multidisciplinary design optimization is required. Work is currently being undertaken to develop an aerostructural framework which incorporates the aerodynamic shape optimization methodology presented here with a finite-element structural solver such that fully coupled aerostructural optimization can be performed.

Acknowledgments

Financial support is provided in part by Bombardier Aerospace under the auspices of the Green Aviation Research and Development Network, the Natural Sciences and Engineering Research Council of Canada, and the University of Toronto. Computations were performed on the General Purpose Cluster supercomputer at the SciNet HPC Consortium. SciNet is funded by: the Canada Foundation for Innovation under the auspices of Compute Canada; the Government of Ontario; Ontario Research Fund - Research Excellence; and the University of Toronto.

References

[1]Liebeck, R., "Design of the Blended Wing Body Subsonic Transport," *Journal of Aircraft*, Vol. 41, No. 1, 2004, pp. 10–25.

[2]Hileman, J. I., Spakovszky, Z. S., Drela, M., Sargeant, M. A., and Jones, A., "Airframe Design for Silent Fuel-Efficient Aircraft," *Journal of Aircraft*, Vol. 47, No. 3, 2010, pp. 956–969.

[3]Li, V. and Velicki, A., "Advanced PRSEUS Structural Concept Design and Optimization," *12th AIAA/ISSMO Multidisciplinary Analysis and Optimization Conference*, AIAA-2008-5840, Victoria, BC, September 2008.

[4]Mukhopadhyay, V., "Blended-Wing-Body Fuselage Structural Design for Weight Reduction," *46th Structures, Structural Dynamics and Materials Conference*, AIAA-2005-2349, Austin, TX, April 2005.

[5]Hansen, L. U., Heinze, W., and Horst, P., "Blended Wing Body Structures in Multidisciplinary Pre-Design," *Structural and Multidisciplinary Optimization*, Vol. 38, No. 1, 2008, pp. 93–106.

[6]Vicroy, D. D., "Blended-Wing-Body Low-Speed Flight Dynamics: Summary of Ground Tests and Sample Results," *47th AIAA Aerospace Sciences Meeting and Exhibit*, AIAA-2009-0933, Orlando, FL, January 2009.

[7]Voskuijl, M., La Rocca, G., and Dircken, F., "Controllability of Blended Wing Body Aircraft," *26th International Congress of the Aeronautical Sciences*, Anchorage, AL, September 2008.

[8]Gern, F. H., "Improved Aerodynamic Analysis for Hybrid Wing Body Conceptual Design Optimization," *50th AIAA Aerospace Sciences Meeting and Exhibit*, AIAA-2012-0249, Nashville, TN, January 2012.

[9]Nickol, C. L., "Hybrid Wing Body Configuration Scaling Study," *50th AIAA Aerospace Sciences Meeting and Exhibit*, AIAA-2012-0337, Nashville, TN, January 2012.

[10]Wakayama, S., "Blended-Wing-Body Optimization Problem Setup," *8th AIAA/USAF/NASA/ISSMO Symposium on Multidisciplinary Analysis and Optimization*, AIAA-2000-4740, Long Beach, CA, September 2000.

[11]Hileman, J. I., Spakovszky, Z. S., Drela, M., and Sargeant, M. A., "Airframe Design for "Silent Aircraft"," *45th AIAA Aerospace Sciences Meeting and Exhibit*, AIAA-2007-0453, Reno, NV, January 2007.

[12]Morris, A. J., "MOB: A European Distributed Multi-Disciplinary Design and Optimisation Project," *9th AIAA/ISSMO Symposium on Multidisciplinary Analysis and Optimization*, AIAA-2002-5444, Atlanta, GA, September 2002.

[13]Méheut, M., Grenon, R., Carrier, G., Defos, M., and Duffau, M., "Aerodynamic Design of Transonic Flying Wing Configurations," *CEAS Katnet II Conference on Key Aerodynamic Technologies*, Breme, Germany, May 2009.

[14]Peigin, S. and Epstein, B., "Computational Fluid Dynamics Driven Optimization of Blended Wing Body Aircraft," *AIAA Journal*, Vol. 44, No. 11, 2006, pp. 2736–2745.

[15]Qin, N., Vavalle, A., Le Moigne, A., Laban, M., Hackett, K., and Weinerfelt, P., "Aerodynamic Considerations of Blended Wing Body Aircraft," *Progress in Aerospace Sciences*, Vol. 40, No. 6, 2004, pp. 321–343.

[16]Le Moigne, A. and Qin, N., "Aerofoil Profile and Sweep Optimisation for a Blended Wing-Body Aircraft Using A Discrete Adjoint Method," *The Aeronautical Journal*, Vol. 110, No. 1111, 2006, pp. 589–604.

[17]Mader, C. A. and Martins, J. R. R. A., "Stability-Constrained Aerodynamic Shape Optimization of Flying Wings," *Journal of Aircraft*, Vol. 50, No. 5, 2013, pp. 1431–1449.

[18]Kuntawala, N. B., Hicken, J. E., and Zingg, D. W., "Preliminary Aerodynamic Shape Optimization Of A Blended-Wing-Body Aircraft Configuration," *49th AIAA Aerospace Sciences Meeting*, AIAA-2011-0642, Orlando, FL, January 2011.

[19]Lyu, Z. and Martins, J. R. R. A., "Aerodynamic Shape Optimization of a Blended-Wing-Body Aircraft," *51st AIAA Aerospace Sciences Meeting*, AIAA-2013-0283, Grapevine, TX, January 2013.

[20]Lyu, Z. and Martins, J. R. R. A., "RANS-based Aerodynamic Shape Optimization of a Blended-Wing-Body Aircraft," *43rd AIAA Fluid Dynamics Conference and Exhibit*, AIAA-2013-2586, San Diego, CA, June 2013.

[21]Reist, T. A. and Zingg, D. W., "Aerodynamic Shape Optimization of a Blended-Wing-Body Regional Transport for a Short Range Mission," *31st AIAA Applied Aerodynamics Conference*, AIAA-2013-2414, San Diego, CA, June 2013.

[22]Hicken, J. E. and Zingg, D. W., "A Parallel Newton-Krylov Solver for the Euler Equations Discretized Using Simultaneous Approximation Terms," *AIAA Journal*, Vol. 46, No. 11, 2008, pp. 2773–2786.

[23]Osusky, M. and Zingg, D. W., "A Parallel Newton-Krylov-Schur Flow Solver for the Navier-Stokes Equations Discretized Using Summation-By-Parts Operators," *AIAA Journal*, Vol. 51, No. 12, 2013, pp. 2833–2851.

[24]Hicken, J. E. and Zingg, D. W., "Aerodynamic Optimization Algorithm with Integrated Geometry Parameterization and Mesh Movement," *AIAA Journal*, Vol. 48, No. 2, 2010, pp. 401–413.

[25]Zingg, D. W., Nemec, M., and Pulliam, T. H., "A Comparative Evaluation of Genetic and Gradient-Based Algorithms Applied to Aerodynamic Optimization," *European Journal of Computational Mechanics*, Vol. 17, No. 1, 2008, pp. 103–126.

[26]Chernukhin, O. and Zingg, D. W., "Multimodality and Global Optimization in Aerodynamic Design," *AIAA Journal*, Vol. 51, No. 6, 2013, pp. 1342–1354.

[27]Hicken, J. E. and Zingg, D. W., "A Simplified and Flexible Variant of GCROT for Solving Nonsymmetric Linear Systems," *SIAM Journal of Scientific Computing*, Vol. 32, No. 3, 2010, pp. 1672–1694.

[28]Gill, P. E., Murray, W., and Saunders, M. A., "SNOPT: An SQP Algorithm for Large-Scale Constrained Optimization," *Society for Industrial Applied Mathematics Review*, Vol. 47, No. 1, 2005, pp. 99–131.

[29]Hicken, J. E. and Zingg, D. W., "Induced Drag Minimization of Nonplanar Geometries Based on the Euler Equations," *AIAA Journal*, Vol. 48, No. 11, 2010, pp. 2564–2575.

[30]Osusky, L. and Zingg, D. W., "Application of an Efficient Newton-Krylov Algorithm for Aerodynamic Shape Optimization Based on the Reynolds-Averaged Navier-Stokes Equations," *21st AIAA Computational Fluid Dynamics Conference*, AIAA-2013-2584, San Diego, CA, June 2013.

[31]Gagnon, H. and Zingg, D. W., "Geometry Generation of Complex Unconventional Aircraft with Application to High-Fidelity Aerodynamic Shape Optimization," *21st AIAA Computational Fluid Dynamics Conference*, AIAA-2013-2850, San Diego, CA, June 2013.

[32]Mozdzanowska, A. and Hansman, R. J., "Evaluation of Regional Jet Operating Patterns in the Continental United States," Tech. Rep. ICAT-2004-1, International Center for Air Transportation, 2004.

[33]Roskam, J., *Airplane Design Part V: Component Weight Estimation*, Aviation and Engineering Corporation, 1989.

[34]Torenbeek, E., *Synthesis of Subsonic Airplane Design*, Delft University, 1976.

[35]Raymer, D. P., *Aircraft Design: A Conceptual Approach*, American Institute of Aeronautics and Astronautics, 5th ed., 2012.

[36]Bradley, K. R., "A Sizing Methodology for the Conceptual Design of Blended-Wing-Body Transports," Tech. Rep. NASA/CR-2004-213016, NASA/Langley Research Center: Joint Institute for Advancement of Flight Sciences, 2004.

[37]Liem, R. P., Mader, C. A., Lee, E., and Martins, J. R. R. A., "Aerostructural Design Optimization of a 100-Passenger Regional Jet with Surrogate-Based Mission Analysis," *13th AIAA Aviation Technology, Integration, and Operations Conference*, AIAA-2013-4372, Los Angeles, CA, August 2013.

[38]Harris, C. D., "NASA Supercritical Airfoils: A Matrix of Family-Related Airfoils," Tech. Rep. NASA TP-2969, NASA, 1990.

[39]Leung, T. and Zingg, D. W., "Aerodynamic Shape Optimization of Wings Using a Parallel Newton-Krylov Approach," *AIAA Journal*, Vol. 50, No. 3, 2012, pp. 540–550.